THE JOURNAL OF PHYSICAL CHEMISTRY B

Article

pubs.acs.org/JPCB

Branching Mechanisms in Surfactant Micellar Growth

Ming Tang*,† and W. Craig Carter‡

†Lawrence Livermore National Laboratory, Livermore, California 94550, United States

‡Massachusetts Institute of Technology, Cambridge, Massachusetts 02139, United States

ABSTRACT: We present a phase-field model to study the morphological transitions of surfactant micelles in supersaturated dilute solution. Simulations reveal that multiply connected micellar structure can be produced by interface branching instability of a growing micelle at relatively large supersaturation and intermediate spontaneous curvatures. Two branching mechanisms, i.e., a disk-to-cylinder shape transition and a tip bifurcation process, are identified for disklike and cylindrical micelles, respectively. We propose that dynamic branching at the micelle growth front provides an important kinetic pathway for the formation of branched wormlike micelles that are observed in many surfactant systems.

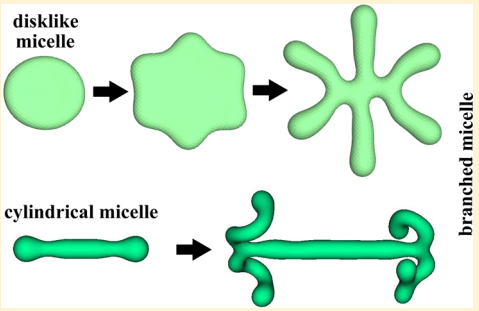

I. INTRODUCTION

At sufficiently large concentrations, amphiphilic molecules such as surfactants can form micellar structures in solutions with three characteristic morphologies: sphere, cylinder, and bilayer. Micelle morphology derives from the bending curvature energy of surfactant layers with an expression introduced by Helfrich[1]

$$E_{curv} = \iint dA[2\kappa(H - H_0)^2 + \bar{\kappa}K] \quad (1)$$

H and K are the mean and Gaussian curvatures of the surfactant layers, and κ and $\bar{\kappa}$ are their corresponding bending moduli. The spontaneous curvature H_0 is an intrinsic property of the surfactant/solvent system that originates from the volume difference between the head and tail groups, and is influenced by parameters such as temperature, electrolyte, and cosurfactants. As H_0 increases, different equilibrium micelle shapes are produced that vary from bilayer to cylindrical and then to spherical morphologies. Although eq 1 was originally derived in the small curvature limit, it has also been applied to evaluate the energetics of the systems with large interface curvature such as surfactant micelles and liquid crystalline phases,[2−4] where the curvature of radius of the interface is comparable to the surfactant chain length, and yields predictions that are consistent with experiments. Bergstrom[5] recently argued that eq 1 provides a quantitative description of the relation between surfactant micelle energy and morphology because the curvature dependence of the main energy terms, e.g., the hydrophobic, electrostatic, and headgroup repulsion contributions, can be adequately approximated by expansion up to second order in H and first order in K.

In addition to spherical, cylindrical, and bilayer structures, other micelle morphologies with nonconstant curvatures are also observed. In particular, experiments reveal the existence of "branched wormlike" micellar networks,[6−11] in which multiple elongated cylinder segments are interconnected by 3-fold "Y-shaped" junctions which have smaller curvatures than the cylindrical body (e.g., see Figure 1a of ref 12). The development of branch points among cylindrical micelles has a significant impact on the rheological properties[13−17] and phase stability of the surfactant solutions.[7] The energetics, thermodynamic stability, and equilibrium properties of the branched junctions and networks have been extensively studied.[12,18−23] However, the kinetic processes that lead to their formation remain much less understood.

Branched wormlike micelles are reminiscent of snow flakes, ramified trees, river deltas, and many other branched structures found in nature. In many cases, dynamic instability of growth fronts produces branching such as in dendritic growth[24] and viscous fingering.[25] Here we use phase-field simulations and linear stability analysis to show that similar interface instability also occurs during micellar growth and produces a branched micelle morphology. Our work emphasizes that micelle shape is not only controlled by thermodynamics but also can be significantly influenced by dynamic instability of the micelle structure, a phenomenon that calls for more modeling and experimental studies in the future.

II. PHASE-FIELD MODEL

The phase-field method, which was first developed for simulating dendritic growth in the solidification process,[24,26,27] has become a powerful tool for modeling a wide range of microstructure evolution phenomena in crystalline materials such as crystal nucleation,[28] grain growth in polycrystals,[29−31] domain structure formation in ferroelectrics,[32−34] sintering of porous structures,[35] electrochemically driven phase transformations in battery electrode materials,[36] etc. In a phase-field model, one or more field variables (or order parameters) are introduced to describe different phases in the system; the spatial locations of the interfaces between different phases are

Received: September 16, 2012
Revised: December 19, 2012
Published: January 30, 2013

implicitly specified by the level sets of the field variables, whose temporal evolution is governed by the Cahn−Hilliard[37] equation for conserved variables or the Allen−Cahn equation[38] for non-conserved variables.

In recent years, phase-field modeling has also found increasing applications in soft matter systems from polymers[39] to membranes[40−42] to monolayers.[43,44] We recently developed a phase-field model for micellar growth in dilute solutions.[45] The model is described below, and a detailed exposition is also available in ref 45.

In a surfactant/polar solvent binary system, a scalar phase-field variable $\phi(\vec{x})$ is introduced to characterize local surfactant concentration and distinguish between the micelle "phase" and the liquid phase. $\phi(\vec{x})$ varies smoothly along a spatial trajectory from −1 at the hydrophobic micelle core to $\phi_{sol} \approx 1$ in solution, where $(1 - \phi_{sol})/2$ represents the volume fraction of free surfactants in solution. The head groups of surfactants are assumed to always abut the polar solvent at the micelle/solution interface specified by the level surface $\phi(\vec{x}) = 0$. The following free energy functional is proposed for the micelle/solution system

$$F[\phi(\vec{x})] = \iiint \left[f(\phi) + \frac{\lambda\sigma^2}{2} p(\phi)^2 - 4\lambda H_0 |\nabla\phi| \nabla^2\phi + \left(\frac{\nu(\phi)}{2} + \lambda\sigma p'(\phi) + 2\lambda {H_0}^2 \right) |\nabla\phi|^2 + \frac{\lambda}{2} (\nabla^2\phi)^2 \right] dV \tag{2}$$

in which the functions $f(\phi)$, $\nu(\phi)$, and $p(\phi)$ will be defined below.

In deriving the free energy functional eq 2, we were motivated by two considerations: (1) It should contain an energy contribution which reduces to eq 1 in the sharp-interface limit to capture the curvature effects on micelle morphology and growth. (2) It should produce stable surfactant aggregates in solution with a characteristic length scale related to the surfactant chain length. To better expose the physics underlying eq 2, we proceed to rewrite it in a local orthogonal coordinate system (r, s, t), where r runs in the direction of $\nabla\phi$ and the surfaces of constant r are the level surfaces of ϕ. s and t are normal to each other and lie in the tangent planes of the ϕ level surfaces. The local r values can be chosen so that $|\partial\vec{x}/\partial r| \equiv |\vec{x}_r| = 1$, where the subscript r denotes the derivative with respect to r. The gradient and Laplacian of $\phi(\vec{x})$ in such a coordinate system have the following expressions:

$$|\nabla\phi| = \left| \frac{\partial\phi}{\partial r} \right| \tag{3}$$

$$\nabla^2\phi = \frac{\partial^2\phi}{\partial r^2} + 2H(r, s, t) \frac{\partial\phi}{\partial r} \tag{4}$$

$H(r, s, t)$ in eq 4 is the mean curvature of the ϕ level surface at (r, s, t). In the local coordinate system, we can show[45] that $H(r, s, t)$ and the Gaussian curvature $K(r, s, t)$ are given by

$$H = \frac{1}{2} \left(\frac{|\vec{x}_s|_r}{|\vec{x}_s|} + \frac{|\vec{x}_t|_r}{|\vec{x}_t|} \right) \tag{5}$$

$$K = \frac{|\vec{x}_s|_r |\vec{x}_t|_r}{|\vec{x}_s||\vec{x}_t|} \tag{6}$$

where $|\vec{x}_s|_r \equiv \partial|\vec{x}_s|/\partial r$ and similarly for $|\vec{x}_t|_r$.

After applying eqs 3 and 4 to eq 2 and changing the variables of integration to $dr\, ds\, dt$, the free energy functional becomes

$$\begin{aligned} F[\phi(\vec{x})] = {} & 2\lambda \iiint dr\, ds\, dt |\vec{x}_s||\vec{x}_t| \left[(H^2 - 4HH_0 + {H_0}^2) \left(\frac{\partial\phi}{\partial r} \right)^2 + (H - 2H_0) \frac{\partial\phi}{\partial r} \frac{\partial^2\phi}{\partial r^2} \right] \\ & + \iiint dr\, ds\, dt |\vec{x}_s||\vec{x}_t| \left[f(\phi) + \frac{\lambda\sigma^2}{2} p(\phi)^2 + \left(\frac{\nu(\phi)}{2} + \lambda\sigma p'(\phi) \right) \left(\frac{\partial\phi}{\partial r} \right)^2 + \frac{\lambda}{2} \left(\frac{\partial^2\phi}{\partial r^2} \right)^2 \right] \\ \equiv {} & F_{curv} + F_{chem} \end{aligned} \tag{7}$$

where the Jacobian for the change of variables is $|\vec{x}_s||\vec{x}_t|$. In eq 7, we divide F into two parts: the first integral, denoted as F_{curv}, depends on the mean curvature of the ϕ level surface and the spontaneous curvature of the system; the second integral, F_{chem}, is curvature-independent. Below, we show that the curvature-dependent energy contribution, F_{curv}, recovers the Helfrich expression in the sharp-interface limit and thus characterizes the bending curvature energy stored in surfactant layers. By applying integration by parts to F_{curv} in eq 7 and using eqs 5 and 6, one obtains[45]

$$F_{curv} = \iiint dr\, ds\, dt |\vec{x}_s||\vec{x}_t| \lambda \left(\frac{\partial\phi}{\partial r} \right)^2 [2(H(\vec{x}) - H_0)^2 - K(\vec{x})] \tag{8}$$

Because $|\partial\phi/\partial r|$ is negligible away from the micelle/solvent interface, eq 8 can be approximated by an integral over the $\phi = 0$ level surface

$$F_{curv} = \iint dA [2\kappa(H - H_0)^2 + \bar{\kappa}K] + O(\xi H) \tag{9}$$

where

$$\kappa = -\bar{\kappa} = \lambda \int_{r_-}^{r_+} \left(\frac{\partial\phi}{\partial r} \right)^2 dr \tag{10}$$

with $r_\pm$ indicating the boundaries of the interfacial region. In the sharp-interface limit where the interface width $\xi \equiv |r_+ - r_-|$ approaches zero, eq 9 shows that F_{curv} reduces to a surface integral over the micelle/solution interface and reproduces eq 1. F_{curv} thus provides a diffuse-interface description of the Helfrich energy. Equation 10 shows that the stiffness of the surfactant monolayer scales with the parameter λ.

The curvature-independent part of the free energy F_{chem} in eq 7 captures the self-assembling tendency of surfactant molecules in solution. Employing integration by parts and assuming $\partial\phi/\partial r = 0$ at $r = \pm\infty$, we rewrite F_{chem} in the following form

dx.doi.org/10.1021/jp309204t | J. Phys. Chem. B 2013, 117, 2898−2905

$$F_{\text{chem}} = \iiint dV\left[f(\phi) + \frac{\nu(\phi)}{2}\left(\frac{d\phi}{dr}\right)^2 + \frac{\lambda}{2}\left(\frac{\partial^2\phi}{\partial r^2} - \sigma p(\phi)\right)^2\right] \quad (11)$$

The physical significance of various terms in eq 11 is described as follows. $f(\phi)$ in eq 11 is the chemical free energy density of a homogeneous surfactant/water solution. Because water and surfactants are immiscible, $f(\phi)$ can be modeled by a double-well-shaped piecewise polynomial

$$f(\phi) = \begin{cases} (\phi^2 - \phi_m^{\,2})^2/(4\phi_m^{\,4}) & |\phi| < \phi_m \\ 100(\phi^2 - \phi_m^{\,2})^2 & |\phi| > \phi_m \end{cases} \quad (12)$$

which has two minima at $\phi = \pm\phi_m \approx \pm 1$ to represent the bulk water and surfactant phases, respectively. Macroscopic phase separation of water and surfactant favored by $f(\phi)$, however, is suppressed by the gradient energy term $1/2\nu(\partial\phi/\partial r)^2$ that has a *negative* gradient coefficient ν within the interfacial region $\phi \approx 0$. A negative gradient energy causes the free energy to decrease by creating surfactant/water interface. The physical justification for this behavior is that an increase in the interface area will expose more hydrophilic head groups of the surfactant molecules to interact favorably with the water molecules, thus reducing the total free energy of the system. On the other hand, ν needs to be positive outside the interfacial region so that the bulk phases remain stable. Following Gompper et al.,[46] this can be satisfied by setting ν as a function of ϕ

$$\nu(\phi) = \nu_0 + (\nu_1 - \nu_0)\phi^2 \quad (13)$$

with $\nu_0 < 0$ and $\nu_1 > 0$. While the interfacial energy is mainly controlled by the value of ν_0, a small positive value can be assigned to ν_1 to guarantee the stability of bulk phases.

If the free energy functional consists of only $f(\phi)$ and the negative gradient energy, the system is unstable and sharp surfactant/water interfaces will form everywhere in the solution. Physically, this cannot happen because the two opposing interfaces on a surfactant aggregate must have a minimal separation that is approximately equal to twice the surfactant chain length. The $\lambda/2(\partial^2\phi/\partial r^2 - \sigma p(\phi))^2$ term in eq 11 introduces an effective interface−interface interaction that gives rise to a stable bilayer structure. Here, $p(\phi)$ is an interpolation function that varies smoothly from $p(-1) = 1$ to $p(1) = 0$. A convenient choice for $p(\phi)$ is

$$p(\phi) = 1/16(1 - \phi)^3(8 + 9\phi + 3\phi^2) \quad (14)$$

The equilibrium bilayer thickness is regulated by the parameter σ in this term. To demonstrate this, consider a plausible bilayer profile

$$\phi_{\text{bilayer}}(r) = \begin{cases} 1 - \frac{32}{l^4}\left(r^2 - \frac{l^2}{4}\right)^2 & -\frac{l}{2} < r < \frac{l}{2} \\ 0 & \text{otherwise} \end{cases} \quad (15)$$

where l specifies the bilayer thickness. Substituting $\phi_{\text{bilayer}}(r)$ into $\lambda/2(\partial^2\phi/\partial r^2 - \sigma p(\phi))^2$ and integrating it between $\pm l/2$, we find that the interaction energy as a function of l has a quadratic form: $F_{\text{bilayer}} = 0.094\lambda\sigma^{5/2}(l - l_{\text{eq}})^2$ + constant near $l = l_{\text{eq}} = 7.24\sigma^{-1/2}$ at which it is minimized. Note that the presence of $p(\phi)$ in the interaction energy ensures that an equilibrium bilayer structure is only characteristic of the surfactant aggregates and does not apply to the solvent.

The derivation of eq 2 was guided by the requirements that the free energy of the system should capture surfactants' self-assembly behavior and the effects of the curvature of surfactant monolayers on micelle free energy, which are essential for studying the morphological stability and evolution of surfactant micelles in solution. In doing so, we constructed a free energy formulation that introduces a surfactant layer−layer interaction to stabilize the characteristic bilayer structure and also reproduces the Helfrich curvature energy in the sharp-interface limit. It should be pointed out that other reasonable choices of the free energy functional that meet these requirements may also exist, and eq 2 may be extended to different surfactant systems to reflect system-specific physics at the molecular level. We note that eq 2 is similar to the Ginzburg−Landau formulation developed by Gompper and co-workers for oil/water/amphiphile ternary systems,[46] but our model explicitly incorporates the spontaneous curvature and introduces a characteristic length scale for the micelle structure. In addition, the free energy form of our model shares features with the phase-field crystal theory[47] which includes a trade-off between negative and positive gradient energy terms that produces a "self-assembly" of ensemble-averaged atoms into crystalline structures.

The time evolution of ϕ is postulated to follow the Cahn−Hilliard equation[37] for conserved order parameters:

$$\frac{\partial\phi}{\partial t} = \nabla\cdot\left[M\nabla\left(\frac{\delta F}{\delta\phi}\right)\right] \quad (16)$$

where M is the mobility of surfactants in solution. For simplicity, we assume that M is a constant and independent of ϕ and interface curvature. Equation 16 simulates the diffusion-controlled micellar growth process. We applied the spectral method to solve eq 16 after nondimensionalizing eqs 2 and 16 with length, energy, and time units $l_c = 2$ nm, $\varepsilon_c = 2.5 \times 10^{-18}$ J, and $t_c = M\varepsilon_c/l_c^3$. The parameters in eq 2 can be fitted to the properties of a specific surfactant/solvent system. Physical quantities are expressed in their dimensionless values hereafter. In all simulations presented here, $\phi_m = 0.999$, $\sigma = 15$, $\nu_0 = -0.075$, $\nu_1 = 0.001$, and $\lambda = 0.005$ are used. They produce a critical micelle concentration of 0.05% volume fraction, bilayer half thickness $l_0 \approx 2$ nm, and bending stiffness $\kappa \approx 20\ kT$, which are similar to the properties of short-chain surfactants like cetyltrimethylammonium bromide (CTAB) in which branched micelles were found to form at increased salt concentrations.[13,14] Nevertheless, we systematically varied the value of H_0 in simulations to examine the effects of spontaneous curvature on micellar growth morphology.

III. RESULTS AND DISCUSSION

We simulated the growth of a spherical micelle nucleus in a supersaturated surfactant solution. The initial concentration of the solution was slightly perturbed from a uniform value. A 64 × 64 × 64 mesh with grid spacing $\Delta x = 10/64$ and periodic boundary conditions was used. As shown in Figure 1, at an initial surfactant concentration $c_0 = 2\%$ volume fraction in solution, the growing micelle's morphology varies from spherical to cylindrical to disklike as H_0 is decreased from $1/l_0$ to $1/2l_0$ and to 0, which conforms to predictions from the curvature energy model. In the case of $H_0 = 0$, the nucleus first

dx.doi.org/10.1021/jp309204t | J. Phys. Chem. B 2013, 117, 2898−2905

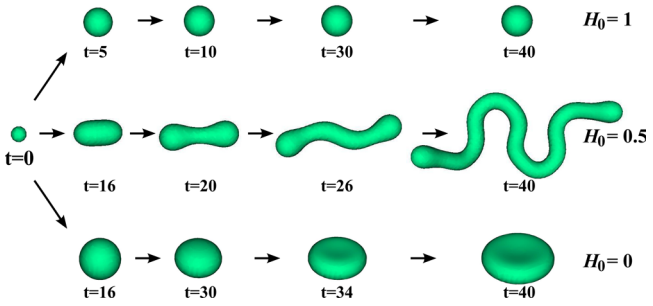

Figure 1. A micelle evolves into the spherical, cylindrical, or disk-like shape under the spontaneous curvature H_0 = 1, 0.5, and 0, respectively, when growing from a spherical nucleus in a solution of c_0 = 2%.

evolves into an intermediate spherical shape before forming a disklike micelle. It is interesting to note that the diameter of the sphere is larger than the thickness of the disk later formed, which at the molecular level may correspond to the surfactant chains being more stretched in a spherical micelle than in a bilayer. This behavior can be explained by the unfavorably large mean curvature of the spherical micelle relative to the spontaneous curvature of the system. The sphere obtains a larger radius to reduce the difference between H and H_0 and thus the curvature energy. For a similar reason, the end-caps of the cylindrical micelle in our simulations also exhibit a larger radius than the cylindrical body (Figure 1). The "swollen" geometry of the end-caps on cylindrical micelles has been previously predicted by theory[48,49] and also observed in cryo-TEM experiments.[7] Our phase-field model appears to be able to qualitatively capture some of the fine features of micellar structures.

Upon increasing supersaturation, however, new micelle growth behavior emerges. We illustrate this by setting H_0 = 0.25—which is intermediate to cylindrical and disklike forms—and comparing micelle evolution behavior at concentration c_0 = 2, 3, and 4%, as shown in Figure 2. For c_0 = 2%, the nucleus grows into a cylindrical micelle. At c_0 = 3%, however, a disklike micelle emerges from the nucleus growth with its radius increasing with time. Nevertheless, the disk's rim becomes unstable at large radii. As shown in Figure 2, perturbation develops at the growth front and generates four finger-like

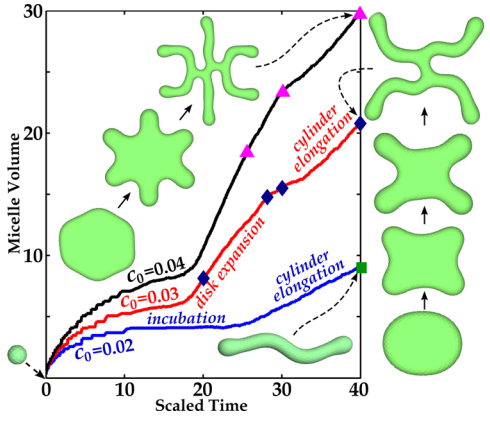

Figure 2. Snapshots of the ϕ = 0 level surface of a micelle growing from a spherical nucleus in solution of c_0 = 2, 3, and 4%, superimposed onto the micelle volume-vs-time plot. The simulation times the snapshots correspond to are marked by a green square for c_0 = 2%, blue diamonds for c_0 = 3%, and pink triangles for c_0 = 4%.

protuberances around t = 28 that subsequently grow by consuming volume from the disk's bilayer region. Eventually, the disklike micelle is transformed into a multiconnected cylindrical micelle with individual arms linked by two 3-fold junctions, a morphology that bears close resemblance to the branched worm-like micelles observed in experiments. Figure 2 also shows the time dependence of micelle volume upon micellar growth. The relatively constant slopes of the micelle volume growth curve in both the disk expansion and cylinder elongation regimes suggest that the disk radius grows as $t^{1/2}$ and the subsequently formed cylindrical branches lengthen at a steady state. A similar morphological transition sequence is also seen at the higher supersaturation c_0 = 4%. Nevertheless, the disk shape instability develops at larger radii with more (six) arms formed at the growth front, producing a branched micelle with four junctions.

Figure 3 shows that the disk-to-cylinder transition behavior observed at c_0 = 3% persists even as H_0 is increased to 0.5,

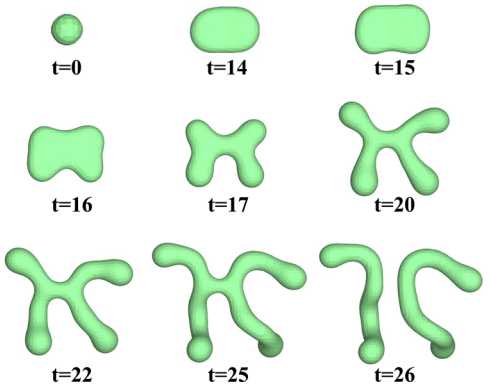

Figure 3. Snapshots of a surfactant micelle with H_0 = 0.5 growing in a solution of c_0 = 3%.

which strongly favors the cylindrical morphology. However, unlike the case of H_0 = 0.25, for H_0 = 0.5, the initially formed branch points become unstable and break up at a later time, resulting in a final configuration of disconnected cylindrical micelles. Therefore, our simulations reveal that two independent conditions are necessary for producing stable branched micelles: (1) an intermediate H_0 between those preferring the disk and cylinder morphologies and (2) a sufficiently large surfactant supersaturation. They are consistent with the experimental observations that a morphological transition from linear to branched wormlike micelles can be induced by increasing surfactant[7] and/or electrolyte concentrations[10,13,14] in solution. The latter has the effect of reducing electrostatic repulsion between head groups of ionic surfactants and lowering the effective spontaneous curvature.

Our simulations suggest that the micelle growth morphology is controlled by the interplay between surfactant supersaturation and the bending curvature energy of surfactant layers. Compared to the one-dimensional growth behavior exhibited at c_0 = 2% for H_0 = 0.25 and 0.5, a larger driving force supplied by the increased supersaturation at c_0 = 3% can overcome the unfavorable curvature-energy and induce a quasi-two-dimensional micelle morphology that facilitates a higher growth rate. However, when free monomers in solution are gradually consumed by disk growth, which causes the driving force to drop, the micelle shape will transform back to the preferred cylindrical geometry under the influence of curvature

dx.doi.org/10.1021/jp309204t | J. Phys. Chem. B 2013, 117, 2898−2905

energy. Such a morphological transition is initiated by the growth front instability of disklike micelles, which is analogous to dendritic growth in solidification of crystalline materials[24] but has not been reported before for surfactant micelles. We show below that the onset of micelle shape instability can be explained by a linear stability analysis similar to the classical Mullins−Serkeka instability[50] for a solidifying growth front.

To analyze stability, we consider diffusion-limited disklike micelle growth in two dimensions. Assume that the initially uniform radius of a disk micelle receives a small perturbation in the form of a sinusoidal wave along the circumference

$$r_d(\theta) = R + \varepsilon \cos(n\theta) \qquad n = 1, 2, 3, \ldots \tag{17}$$

where $0 < \varepsilon \ll R$ and $R \gg l_0$. We assume that the micelle consists only of surfactant molecules. Let c_0 be the surfactant monomer concentration in solution far from the micelle and c_{eq} the concentration at the disk front that is in local equilibrium with the micelle. If the solution is supersaturated, i.e., $c_0 > c_{eq}$, a surfactant monomer flux toward the micelle is generated by the concentration gradient, which causes the micelle to grow.

Let $\Delta\mu$ be the excess chemical potential of a surfactant molecule in the disk's rim relative to a monomer in the flat bilayer, which serves as a reference state. Analogous to the Gibbs−Thomson equation that accounts for the dependence of the local chemical potential on the surface energy, we can relate $\Delta\mu$ to the bending curvature energy associated with the disk's rim

$$\Delta\mu = \Omega \frac{\delta \Delta E_{curv}^{rim}}{\delta V} \tag{18}$$

where Ω is the volume of a monomer and V the volume of the disk micelle defined by

$$V = l_0 \int_0^{2\pi} r_d(\theta)^2 \, d\theta \tag{19}$$

E_{curv}^{rim} is the bending curvature energy of the disk's rim and given by

$$\Delta E_{curv}^{rim} = \frac{\pi \kappa l_0}{2} \int_0^{2\pi} (\chi^r - \chi_0^r)^2 \sqrt{r_d(\theta)^2 + r_d'(\theta)^2} \, d\theta \tag{20}$$

where

$$\chi^r = \frac{(r_d(\theta)^2 + 2r_d'(\theta)^2 - r_d(\theta) r_d''(\theta))^2}{(r_d(\theta)^2 + r_d'(\theta)^2)^{3/2}} \tag{21}$$

is the rim's radial curvature[51] and $\chi_0^r \equiv 2H_0 - 1/l_0$ is the preferred radial curvature. Using eq 19 and the equality $\delta\Delta E_{curv}^{rim}/\delta V = (\delta\Delta E_{curv}^{rim}/\delta r_d(\theta))/(\delta V/\delta r_d(\theta))$, eq 18 can be rewritten as

$$\Delta\mu = \frac{\Omega}{2 l_0 r_d(\theta)} \frac{\delta \Delta E_{curv}^{rim}}{\delta r_d(\theta)} \tag{22}$$

Because the micelle and the solution are in local equilibrium at the interface, $\Delta\mu$ can also be written as

$$\Delta\mu = kT \ln\left(\frac{c_{eq}}{c_{eq}^0}\right) \tag{23}$$

in the dilute solution limit, where c_{eq}^0 is the surfactant concentration of the solution in equilibrium with the flat surfactant bilayer. Combining eqs 22 and 23, we obtain

$$c_{eq}(\theta) = c_{eq}^0 \exp\left(\frac{\Omega}{2kTl_0 r_d(\theta)} \frac{\delta \Delta E_{curv}^{rim}}{\delta r_d(\theta)}\right) \approx c_{eq}^0 \left(1 + \frac{\Omega}{2kTl_0 r_d(\theta)} \frac{\delta \Delta E_{curv}^{rim}}{\delta r_d(\theta)}\right) \tag{24}$$

which defines the boundary condition for the diffusion equation of surfactant in solution at the micelle interface.

At $r \gg R$, (r the radial distance from the disk center), i.e. far from the disk, the concentration flux in solution is determined to be

$$\left.\frac{\partial c}{\partial r}\right|_{r \gg R} = \frac{2(c_0 - c_{eq})}{|\ln \Delta\bar{C}| r} \tag{25}$$

from the self-similarity solution of the diffusion equation.[24] In the small supersaturation limit $\Delta\bar{C} \equiv (c_0 - c_{eq})/(1 - c_{eq}) \ll 1$, surfactant diffusion in front of the disk can be assumed to be quasi-steady-state and obey the Laplace equation, $\nabla^2 c = 0$. By solving the Laplace equation with the boundary conditions eqs 24 and 25, the surfactant concentration gradient at the disk/solution interface can be determined and the disk's growth velocity can be evaluated according to the Stefan condition:[52]

$$\frac{dr_d(\theta)}{dt} = \frac{dR}{dt} + \frac{d\varepsilon}{dt}\cos(n\theta) = \frac{D}{1 - c_{eq}} \left.\frac{\partial c}{\partial r}\right|_{r = r_d(\theta)} \tag{26}$$

We obtain from eq 26

$$\frac{dR}{dt} = \frac{2D}{|\ln \Delta\bar{C}|} \frac{1}{R} \tag{27}$$

which explains the parabolic growth of the disk radius (or the linear growth of the disk volume) seen in Figure 2. The growth rate of the perturbation amplitude is found to be

$$\frac{d\varepsilon}{dt} = \frac{D(n-1)}{(1 - c_{eq})R}\left[\frac{2(c_0 - c_{eq})}{|\ln \Delta\bar{C}|R} - \frac{\pi\kappa\Omega c_0}{4kT} \frac{n(n+1)[2n^2 - 3 + (2\chi_0^r R)^2]}{R^3}\right] \tag{28}$$

Whether the perturbation will grow or diminish depends on the sign of $d\varepsilon/dt$. The first term within the brackets on the right-hand side of eq 28 scales with R^{-1}, and the second term scales with $-R^{-3}$. Therefore, for any given wavenumber $n > 1$, a disk micelle will eventually become unstable (i.e., $d\varepsilon/dt > 0$) against the perturbation when its radius R becomes sufficiently large. The critical radius above which $d\varepsilon/dt > 0$ and thus the interface instability develops is both n- and H_0-dependent. At a given radius R, the perturbation growth rate $d\varepsilon/dt$ is also n- and H_0-dependent. According to eq 28, the fastest growing perturbation mode at a fixed H_0 has a wavenumber n_{max} that scales with $R^{3/4}$ in a cylinder-favoring system (i.e., $H_0 = 1/2l_0$ or $\chi_0^r = 0$), or $n_{max} \propto R^{1/2}$ when the bilayer morphology is preferred (i.e., $H_0 \to 0$). The R dependence of n_{max} explains why more cylindrical fingers emerge from the disk's rim when the initial solution concentration c_0 is increased from 3 to 4% in our simulations (Figure 2): at the higher supersaturation c_0 = 4%, R has a larger growth rate because of the increased driving force. As a result, the growth of perturbation is not significant relative to uniform disk expansion until reaching a larger R, at which the dominant perturbation has a larger n_{max} and more protuberances are thus generated than in the case of c_0 = 3%.

dx.doi.org/10.1021/jp309204t | J. Phys. Chem. B 2013, 117, 2898−2905

In addition to the disk instability, we discovered from simulations that branching can also occur to cylindrical micelles via a tip splitting mechanism. Figure 4 shows a cylindrical micelle with H_0 = 0.25 that was first grown from a spherical nucleus at c_0 = 2%, and subsequently subject to a higher monomer concentration at c_0 = 3%. After the solution concentration change, the spherical cap of the cylindrical micelle starts to swell because the increased supersaturation causes surfactant monomers to be absorbed into the micelle growth front more rapidly than can be accommodated by the cylinder elongation. However, the larger cap is not favored by the curvature energy, and it gradually flattens and then splits into two smaller caps, leaving a Y-shaped junction behind. The morphological transition consumes surfactant monomers in the region surrounding the cap and reduces the local supersaturation. The newly formed arms thus grow into two cylindrical branches after splitting. As shown in Figure 4, tip splitting may happen again when the cylinder caps enter regions with sufficiently high surfactant concentration. This phenomenon resembles the tip splitting of a needle crystal in the absence of surface energy anisotropy,[24] but here it is the bending curvature energy rather than the surface energy that dampens the interface perturbation. The onset of tip splitting in a cylindrical micelle can be analyzed by a linear stability analysis similar to that for crystal growth[24] and will be reported elsewhere.

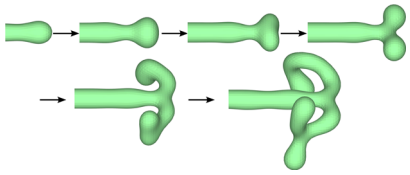

Figure 4. Snapshots of a cylindrical micelle with H_0 = 0.25 growing in solution of c_0 = 3% at t = 0, 15, 20, 23, 31, and 36. Only half of the micelle is shown for clarity.

The tip bifurcation process provides a mechanism for a single micelle to repeatedly add branch points to itself to sprawl into a hierarchically branched network structure. We demonstrate this point with a micelle growth simulation using H_0 = 0.25 and c_0 = 3% and a computation domain of size 40 × 40 × 40 that is much larger than those used in Figures 2 and 4. As shown in Figure 5, after two junctions emerge from the disk front perturbation of n = 4, more junctions are generated by tip bifurcation at the growth front, which result in a multiconnected branched wormlike micelle at the end of simulation. We note that the reason that multiple branching events can occur subsequently in this simulation but not in simulations using smaller domain sizes is that the solution supersaturation decreases more slowly with time upon micellar growth in the larger computation box and the driving force remains sufficiently high for interface instability to develop over an extended period of time.

The effect of convection in solution on micellar growth is not considered in the current model. Our model can be extended to incorporate hydrodynamic effects by coupling the phase field to velocity field as done in the phase-field modeling of vesicle dynamics.[42] Similar to dendritic crystal growth,[53] we expect that hydrodynamic flow can significantly modify the branching patterns of micelles, but diffusion-limited transport remains a fundamental contributor to the branching instability.

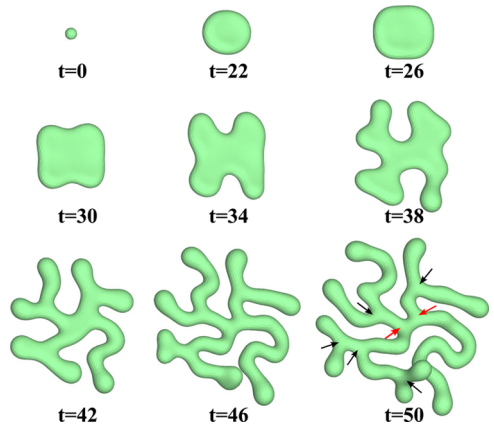

Figure 5. Snapshots of a micelle with H_0 = 0.25 growing from a spherical nucleus in a solution of c_0 = 3%, using a large computation domain (see text). Branching junctions formed from disk-to-cylinder transition are marked by red arrows, and those generated by tip bifurcation are highlighted by black arrows on the micelle snapshot at t = 50.

IV. CONCLUSION

In conclusion, results from phase-field simulations and linear stability analysis provide the first evidence that links the development of branched wormlike micelles to micelle/solution interface instability during micellar growth. Branch points can develop through disk-to-cylinder or tip-splitting morphological transitions, which lead to the formation of multiply connected network structures. In micellar systems, the equilibrium between micelles and the surrounding solution is dynamically maintained through constant exchange of surfactant molecules between them. Surfactant monomer concentration in the solution exhibits significant fluctuation both spatially and temporally, and branching instability can occur to micelles in regions with large local supersaturation. While the stability of the as-formed junctions is ultimately determined by the thermodynamic properties of the surfactant/solvent systems, the dynamic branching phenomena revealed in this work provide an important kinetic mechanism for establishing the equilibrium junction density in the micellar networks. Although recent progress in experimental techniques has considerably enriched our knowledge of branched micelle structures, it remains a challenging task to infer the details of branching dynamics from experimental observations. We demonstrate in this paper that phase-field simulation is a useful tool to compliment experiments to provide valuable insights on the morphological evolution of surfactant self-assembled structures.

AUTHOR INFORMATION

Corresponding Author

*E-mail: mingtang@alum.mit.edu.

Notes

The authors declare no competing financial interest.

ACKNOWLEDGMENTS

M.T. acknowledges financial support from the Lawrence Postdoctoral Fellowship and the Laboratory Directed Research and Development Program under the auspices of the U.S. Department of Energy by Lawrence Livermore National Laboratory under Contract DE-AC52-07NA27344. W.C.C. was supported by the National Science Foundation under

Grant No. DMR-0906931. Part of the simulations were carried out at the National Energy Research Scientific Computing Center, which is supported by the Office of Science of the U.S. Department of Energy under Contract No. DE-AC02-05CH11231.

REFERENCES

(1) Helfrich, W. Elastic Properties of Lipid Bilayers - Theory and Possible Experiments. *Z. Naturforsch., C* **1973**, *28*, 693−703.
(2) Kozlov, M. M.; Leikin, S.; P., R. R. Bending, Hydration and Interstitial Energies Quantitatively Account for the Hexagonal-Lamellar-Hexagonal Reentrant Phase Transition in Dioleoylphosphatidylethanolamine. *Biophys. J.* **1994**, *67*, 1603−1611.
(3) Roth, Y.; Opatowski, E.; Lichtenberg, D.; Kozlov, M. M. Phase Behavior of Dilute Aqueous Solutions of Lipid-Surfactant Mixtures: Effects of Finite Size of Micelles. *Langmuir* **2000**, *16*, 2052−2061.
(4) Johansson, E.; Sandstrom, M. C.; Bergstrom, M.; Edwards, K. On the Formation of Discoidal versus Threadlike Micelles in Dilute Aqueous Surfactant/Lipid Systems. *Langmuir* **2008**, *24*, 1731−1739.
(5) Bergstrom, L. M. Bending Energetics of Tablet-Shaped Micelles: A Novel Approach to Rationalize Micellar Systems. *ChemPhysChem* **2007**, *8*, 462−472.
(6) Danino, D.; Talmon, Y.; Levy, H.; Beinert, G.; Zana, R. Branched Thread-Like Micelles in an Aqueous-Solution of a Trimeric Surfactant. *Science* **1995**, *269*, 1420−1421.
(7) Bernheim-Groswasser, A.; Zana, R.; Talmon, Y. Sphere-to-Cylinder Transition in Aqueous Micellar Solution of a Dimeric (Gemini) Surfactant. *J. Phys. Chem. B* **2000**, *104*, 4005−4009.
(8) Bernheim-Groswasser, A.; Tlusty, T.; Safran, S. A.; Talmon, Y. Direct Observation of Phase Separation in Microemulsion Networks. *Langmuir* **1999**, *15*, 5448−5453.
(9) Bernheim-Groswasser, A.; Wachtel, E.; Talmon, Y. Micellar Growth, Network Formation, and Criticality in Aqueous Solutions of the Nonionic Surfactant C12E5. *Langmuir* **2000**, *16*, 4131−4140.
(10) Croce, V.; Cosgrove, T.; Maitland, G.; Hughes, T.; Karlsson, G. Rheology, Cryogenic Transmission Electron Spectroscopy, and Small-Angle Neutron Scattering of Highly Viscoelastic Wormlike Micellar Solutions. *Langmuir* **2003**, *19*, 8536−8541.
(11) Flood, C.; Dreiss, C. A.; Croce, V.; Cosgrove, T. Wormlike Micelles Mediated by Polyelectrolyte. *Langmuir* **2005**, *21*, 7646−7652.
(12) Tlusty, T.; Safran, S. A.; Strey, R. Topology, Phase Instabilities, and Wetting of Microemulsion Networks. *Phys. Rev. Lett.* **2000**, *84*, 1244−1247.
(13) Khatory, A.; Lequeux, F.; Kern, F.; Candau, S. J. Linear and Nonlinear Viscoelasticity of Semidilute Solutions of Wormlike Micelles at High-Salt Content. *Langmuir* **1993**, *9*, 1456−1464.
(14) Oelschlaeger, C.; Suwita, P.; Willenbacher, N. Effect of Counterion Binding Efficiency on Structure and Dynamics of Wormlike Micelles. *Langmuir* **2010**, *26*, 7045−7053.
(15) Schubert, B. A.; Kaler, E. W.; Wagner, N. J. The Microstructure and Rheology of Mixed Cationic/Anionic Wormlike Micelles. *Langmuir* **2003**, *19*, 4079−4089.
(16) In, M.; Warr, G. G.; Zana, R. Dynamics of Branched Threadlike Micelles. *Phys. Rev. Lett.* **1999**, *83*, 2278−2281.
(17) Magid, L. J. The Surfactant-Polyelectrolyte Analogy. *J. Phys. Chem. B* **1998**, *102*, 4064−4074.
(18) Porte, G.; Gomati, R.; El Haitadmy, O.; Appell, J.; Marignan, J. Morphological Transformations of the Primary Surfactant Structures in Brine-Rich Mixtures of Ternary Systems (Surfactant/Alcohol/Brine). *J. Phys. Chem.* **1986**, *90*, 5746−5751.
(19) Drye, T. J.; Cates, M. E. Living Networks - the Role of Cross-Links in Entangled Surfactant Solutions. *J. Chem. Phys.* **1992**, *96*, 1367−1375.
(20) May, S.; Bohbot, Y.; BenShaul, A. Molecular Theory of Bending Elasticity and Branching of Cylindrical Micelles. *J. Phys. Chem. B* **1997**, *101*, 8648−8657.
(21) Andreev, V. A.; Victorov, A. I. Molecular Thermodynamics for Micellar Branching in Solutions of Ionic Surfactants. *Langmuir* **2006**, *22*, 8298−8310.
(22) Tlusty, T.; Safran, S. A. Defect-Induced Phase Separation in Dipolar Fluids. *Science* **2000**, *290*, 1328−1331.
(23) Zilman, A. G.; Safran, S. A. Thermodynamics and Structure of Self-Assembled Networks. *Phys. Rev. E* **2002**, *66*, 051107.
(24) Karma, A. *Branching in Nature*; Springer: Berlin, 2001; Chapter XI, pp 365−401.
(25) Saffman, P. G.; Taylor, G. The Penetration of a Fluid into a Porous Medium or Hele-Shaw Cell Containing a More Viscous Liquid. *Proc. R. Soc. London, Ser. A* **1958**, *245*, 312−329.
(26) Boettinger, W. J.; Warren, J. A.; Beckermann, C.; Karma, A. Phase-Field Simulation of Solidification. *Annu. Rev. Mater. Res.* **2002**, *32*, 163−194.
(27) Haxhimali, T.; Karma, A.; Gonzales, F.; Rappaz, M. Orientation Selection in Dendritic Evolution. *Nat. Mater.* **2006**, *5*, 660−664.
(28) Toth, G. I.; Granasy, L. Crystal Nucleation in the Hard-Sphere System Revisited: A Critical Test of Theoretical Approaches. *J. Phys. Chem. B* **2009**, *113*, 5141−5148.
(29) Chen, L.-Q.; Yang, W. Computer Simulation of the Domain Dynamics of a Quenched System with a Large Number of Nonconserved Order Parameters: The Grain-Growth Kinetics. *Phys. Rev. B* **1994**, *50*, 15752−15758.
(30) Warren, J. A.; Kobayashi, R.; Lobkovsky, A. E.; Carter, W. Extending Phase Field Models of Solidification to Polycrystalline Materials. *Acta Mater.* **2003**, *51*, 6035−6058.
(31) Tang, M.; Reed, B. W.; Kumar, M. Coarsening Kinetics of Topologically Highly Correlated Grain Boundary Networks. *J. Appl. Phys.* **2012**, *112*, 043505.
(32) Li, Y. L.; Hu, S. Y.; Liu, Z. K.; Chen, L. Q. Phase-Field Model of Domain Structures in Ferroelectric Thin Films. *Appl. Phys. Lett.* **2001**, *78*, 3878−3880.
(33) Li, Y. L.; Hu, S. Y.; Liu, Z. K.; Chen, L. Q. Effect of Substrate Constraint on the Stability and Evolution of Ferroelectric Domain Structures in Thin Films. *Acta Mater.* **2002**, *50*, 395−411.
(34) Vasudevan, R. K.; Chen, Y.-C.; Tai, H.-H.; Balke, N.; Wu, P.; Bhattacharya, S.; Chen, L.-Q.; Chu, Y.-H.; Lin, I.-N.; Kalinin, S. V.; Nagarajan, V. Exploring Topological Defects in Epitaxial BiFeO3 Thin Films. *ACS Nano* **2011**, *5*, 879−887.
(35) Mukherjee, R.; Chakrabarti, T.; Anumol, E. A.; Abinandanan, T. A.; Ravishankar, N. Thermal Stability of Spherical Nanoporous Aggregates and Formation of Hollow Structures by Sintering — A Phase-Field Study. *ACS Nano* **2011**, *5*, 2700−2706.
(36) Tang, M.; Belak, J. F.; Dorr, M. R. Anisotropic Phase Boundary Morphology in Nanoscale Olivine Electrode Particles. *J. Phys. Chem. C* **2011**, *115*, 4922−4926.
(37) Cahn, J. W. On Spinodal Decomposition. *Acta Metall.* **1961**, *9*, 795−801.
(38) Allen, S. M.; Cahn, J. W. A Microscopic Theory for Antiphase Boundary Motion and Its Application to Antiphase Domain Coarsening. *Acta Metall.* **1979**, *27*, 1085−1095.
(39) Granasy, L.; Pusztai, T.; T., B.; Warren, J. A.; Douglas, J. F. A General Mechanism of Polycrystalline Growth. *Nat. Mater.* **2004**, *3*, 645−650.
(40) Du, Q.; Liu, C.; Wang, X. A Phase Field Approach in the Numerical Study of the Elastic Bending Energy for Vesicle Membranes. *J. Comput. Phys.* **2004**, *198*, 450−468.
(41) Jamet, D.; Misbah, C. Towards a Thermodynamically Consistent Picture of the Phase-Field Model of Vesicles: Local Membrane Incompressibility. *Phys. Rev. E* **2007**, *76*, 051907.
(42) Biben, T.; Kassner, K.; Misbah, C. Phase-Field Approach to Three-Dimensional Vesicle Dynamics. *Phys. Rev. E* **2005**, *72*, 041921.
(43) Lu, W.; Kim, D. Patterning Nanoscale Structures by Surface Chemistry. *Nano Lett.* **2004**, *4*, 313−316.
(44) Zhao, M.; Deng, K.; Jiang, P.; Xie, S.-S.; Fichou, D.; Jiang, C. Binary-Component Self-Assembled Monolayer Comprising Tetrathiafulvalene and n-Tetradecane Molecules with Periodic Ordered Phase

Separation Structures on a Highly Oriented Pyrolytic Graphite Surface. *J. Phys. Chem. C* **2010**, *114*, 1646−1650.
(45) Tang, M. Thermodynamic and Morphological Transitions in Crystalline and Soft Material Interfaces. Ph.D. thesis, MIT, 2008.
(46) Gompper, G.; Schick, M. Correlation Between Structural and Interfacial Properties of Amphiphilic Systems. *Phys. Rev. Lett.* **1990**, *65*, 1116−1119.
(47) Elder, K. R.; Katakowski, M.; Haataja, M.; M., G. Modeling Elasticity in Crystal Growth. *Phys. Rev. Lett.* **2002**, *88*, 245701.
(48) Eriksson, J. C.; Ljunggren, S. The Mechanics and Thermodynamics of Rod-Shaped Micelles. *J. Chem. Soc., Faraday Trans. 2* **1985**, *81*, 1209−1242.
(49) Eriksson, J. C.; S., L. Model Calculations on the Transitions between Surfactant Aggregates of Different Shapes. *Langmuir* **1990**, *6*, 895−904.
(50) Mullins, W. W.; Sekerka, R. F. Morphological Stability of a Particle Growing by Diffusion or Heat Flow. *J. Appl. Phys.* **1963**, *34*, 323−329.
(51) Gray, A. *Modern Differential Geometry of Curves and Surfaces with Mathematica*, 2nd ed.; CRC Press: Boca Raton, FL, 1997; pp 89−89.
(52) Balluffi, R. W.; Allen, S. M.; Carter, W. C. *Kinetics of Materials*; Wiley: New York, 2005.
(53) Tong, X.; Beckermann, C.; Karma, A.; Li, Q. Phase-Field Simulations of Dendritic Crystal Growth in a Forced Flow. *Phys. Rev. E* **2001**, *63*, 061601.